



## Precise control of intracycle interference with a phase-stabilized polarization-gated laser pulse

RenPing Sun,<sup>1,\*</sup> YanLan Wang,<sup>1,2,\*</sup> Yu Zhou,<sup>1,2</sup> ShaoGang Yu <sup>1</sup>, SongPo Xu,<sup>1</sup> XuanYang Lai,<sup>1,2</sup>  
Wei Quan <sup>1,2,†</sup> and XiaoJun Liu<sup>1,2,‡</sup>

<sup>1</sup>State Key Laboratory of Magnetic Resonance and Atomic and Molecular Physics, Wuhan Institute of Physics and Mathematics, Innovation Academy for Precision Measurement Science and Technology, Chinese Academy of Sciences, Wuhan 430071, China

<sup>2</sup>University of Chinese Academy of Sciences, Beijing 100049, China



(Received 18 August 2021; accepted 28 January 2022; published 16 February 2022)

We investigate photoelectron momentum distribution (PMD) from strong-field ionization of Ar by a polarization-gated (PG) pulse constructed by a left circularly polarized and a time-delayed right circularly polarized carrier-envelope phase stabilized few-cycle laser pulse. We experimentally demonstrate the feasibility of using a PG pulse to precisely control the interferences between electron wave packets (EWPs) released at different times within one optical cycle. In contrast to previous works where the various types of intracycle interferences are usually hardly resolved and separated, our work shows that, with this specific PG control scheme, it becomes possible to create a highly distinct interference pattern composed of well-separated structures produced by different types of intracycle interferences in the measured PMD. Quantum trajectory Monte Carlo simulations reproduce well the experimental findings and uncover the physical mechanism behind this subcycle control of EWPs with a PG pulse.

DOI: [10.1103/PhysRevA.105.L021103](https://doi.org/10.1103/PhysRevA.105.L021103)

### I. INTRODUCTION

Interference lies at the heart of quantum mechanics. The most conceptually important interference experiment is the double-slit scheme, which was first demonstrated with the light wave, well known as Young's double-slit experiment over the centuries and later on extensively expanded to matter waves by, e.g., electron diffraction [1–3]. In recent years, a versatile scenario of the double-slit interference effects has been identified via strong-field and attosecond physics studies [4–16]. Therein an atom or a molecule is tunnel ionized in an intense femtosecond laser field, creating ultrashort electron wave packets (EWPs) at different times or different positions [17,18]. The emitted wave packets with the same final momentum will interfere with each other, creating rich interference features in the final photoelectron momentum distribution (PMD), which contains a wealth of information about the structure and ultrafast dynamics of the system [19–23].

The most prominent EWP interference in strong-field ionization is the intercycle interference, for which the repetitive EWPs released at a time interval of one optical cycle interfere with each other, forming the well-known above-threshold ionization (ATI) peaks in the PMD [24,25]. In addition, there are several types of interference that originate from EWPs emitted within one laser cycle, including intracycle interference produced by the direct EWPs emitted from adjacent

or nonadjacent quarter cycles of the laser pulse [26–28] and the photoelectron holography (PH) that originates from interference of the direct and the laser-driven rescattering EWPs [19,29–31]. In particular, intracycle interference has attracted much attention recently since it could provide deep insight into the attosecond electronic dynamics during the tunneling ionization process [32–34]. However, in order to accurately extract attosecond electronic dynamics from intracycle interference, one needs to clearly resolve and separate various intracycle interference patterns in the PMD, which are always buried in a wealth of other more prominent structures, e.g., intercycle interference and PH structures. Several experimental schemes have been attempted to achieve this goal. Early experimental works [4,35] have demonstrated that a few-cycle laser pulse can be used to suppress the intercycle interference and to distinguish the identifying characteristic of the intracycle interference. However, in this scheme, different intracycle interference and pronounced forward-rescattering PH patterns are strongly mixed in the PMD [36]. Recently, an orthogonally polarized two-color (OTC) pulse has been employed to separate different intracycle interferences in the PMD [27,37]. Nevertheless, for the multicycle characteristic of the OTC field employed so far, the intercycle interference unavoidably contributes a strong background and smears out the intracycle interference structures heavily.

In this paper we employ a polarization-gated (PG) pulse consisting of two counterrotating circularly polarized and carrier-envelope phase (CEP) stabilized few-cycle laser pulses, to demonstrate experimentally subcycle precise control of the intracycle interferences. The key to achieve this goal relies on the strong dependence of the attosecond electron wave-packet dynamics on the subcycle shape of

\*These authors contributed equally to this work.

†charlywing@wipm.ac.cn

‡xjliu@wipm.ac.cn

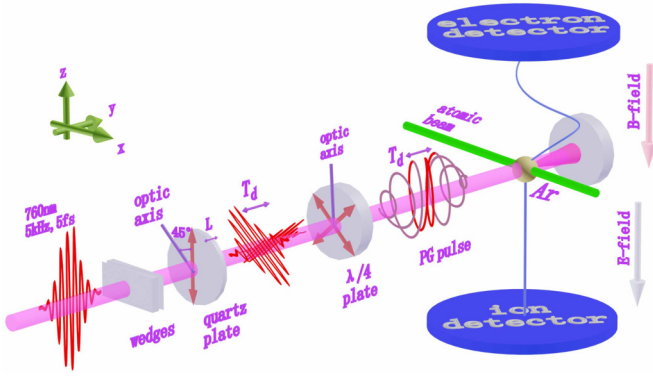


FIG. 1. Schematic of the experimental setup (see the text for a description).

the electric field of the PG pulse, which can be precisely controlled by the time delay and CEP of the combining few-cycle pulses [38–42]. With the controllable PG laser field, we are able to suppress the intercycle interference and the forward-rescattering PH structures and create a highly distinct interference pattern which is composed of well-separated structures caused by different types of intracycle interferences in the PMD. Note that the PG pulse has been successfully used in the generation of isolated attosecond pulses by the effective control of EWP dynamics with subcycle temporal resolution [40,41,43]. However, in that case, the rescattered electron plays a major role in the strong-field process, which frustrates a straightforward understanding of the subcycle manipulation. In contrast, by extracting unambiguously the intracycle interferences from direct electron wave packets in the PMD, our work provides a more distinct scheme of subcycle control of electron dynamics.

## II. EXPERIMENTAL SETUP

The experimental setup is shown schematically in Fig. 1. In our experiment, femtosecond linearly polarized laser pulses are generated from a commercial Ti:sapphire femtosecond laser system with a repetition rate of 5 kHz, a pulse duration around 30 fs, and a center wavelength of 800 nm. The laser pulses from the commercial laser system are spectrally broadened in a neon-filled hollow fiber and subsequently compressed by several pairs of chirped mirrors down to a duration as short as 5 fs with a center wavelength of 760 nm. The laser pulse energy can be controlled by neutral density filters. The CEP of the few-cycle pulse is stabilized utilizing a monolithic stabilization scheme for the oscillator [44] while slow phase drifts imparted to the pulses in the amplification process are compensated by an  $f$ - $2f$  interferometer [45]. The CEP can be adjusted by a pair of fused silica wedges. A birefringent quartz plate of specified thickness and an achromatic  $\lambda/4$  plate are used to generate a pair of counterrotating, time-delayed circularly polarized few-cycle pulses and realize the PG laser pulse [40]. The time delay  $T_d$  between these two circularly polarized pulses can be controlled by changing the thickness of the birefringent quartz plate. It is estimated that a thickness of 0.1 mm causes a time delay of about 3 fs.

The measurement is performed using a cold target recoil ion momentum spectroscopy (COLTRIMS) [46–49]. The phase-stabilized PG laser pulses are focused by an on-axis spherical mirror ( $f = 75$  mm) onto a cold supersonic gas jet inside the COLTRIMS vacuum chamber. The created ions and electrons are accelerated by a uniform electric field of 5.0 V/cm towards the ion and electron position-sensitive microchannel plate detectors equipped with delay line anodes. A pair of Helmholtz coils generates a uniform magnetic field of 3.9 G to confine the electron movement perpendicular to the electric field. From the recorded time of flight and impact position on the detector, the three-dimensional momenta of each particle can be retrieved. We measure the three-dimensional momenta of the photoelectrons produced in coincidence with the singly charged ions of Ar. In our experiment, the CEP of the few-cycle pulse is calibrated by the asymmetry of the measured  $\text{Ar}^+$  momentum distribution [35] and the intensity of the few-cycle pulse is calibrated with a procedure utilizing the photoelectron momentum distribution in a close to circularly polarized laser field [50].

## III. RESULTS

The electric-field components of the PG pulse in the polarization plane (i.e., in the  $z$  and  $x$  directions) can be expressed as

$$E_z(t) = E_0 \left[ \cos^2 \left( \frac{\omega(t - T_d/2)}{2n} \right) + \cos^2 \left( \frac{\omega(t + T_d/2)}{2n} \right) \right] \times \cos(\omega t + \varphi) \quad (1)$$

and

$$E_x(t) = E_0 \left[ -\cos^2 \left( \frac{\omega(t - T_d/2)}{2n} \right) + \cos^2 \left( \frac{\omega(t + T_d/2)}{2n} \right) \right] \times \sin(\omega t + \varphi), \quad (2)$$

where  $E_0$  is the maximum electric-field amplitude of the left or right circularly polarized few-cycle pulse,  $\omega$  is the laser angular frequency,  $T_d$  is the time delay between two pulses, and  $\varphi$  is the CEP of the two pulses, with  $n = 6$  the number of optical cycles for each circularly polarized laser pulse. Figures 2(a)–2(d) show the electric-field components in the  $z$  and  $x$  directions and the ellipticity of the PG pulses for different time delay and CEP combinations, denoted by  $(T_d, \varphi)$ , where  $T_d = nT$  and  $T$  is the optical period of the few-cycle pulse. As shown in Figs. 2(a)–2(c), the time delay  $T_d$  has a strong influence on the ellipticity of the combined laser field. When  $T_d = 0$ , the PG pulse becomes a linearly polarized pulse. As  $T_d$  increases, the ellipticity of the PG pulse becomes time dependent; it is circularly polarized at the edges of the pulse and becomes approximately linearly polarized, i.e.,  $\varepsilon < 0.2$  (see blue boxes in Fig. 2), in the vicinity of  $t = 0$ . A longer time delay corresponds to a sharper slope and thus a narrower linear gating. In contrast to the time delay, as shown in Fig. 2(d), the variation of the CEP only modifies the temporal shape of the combined electric field, but hardly changes the ellipticity of the PG pulse.

Figures 2(e)–2(h) show the measured PMDs in the polarization plane of the PG laser pulse for the combinations

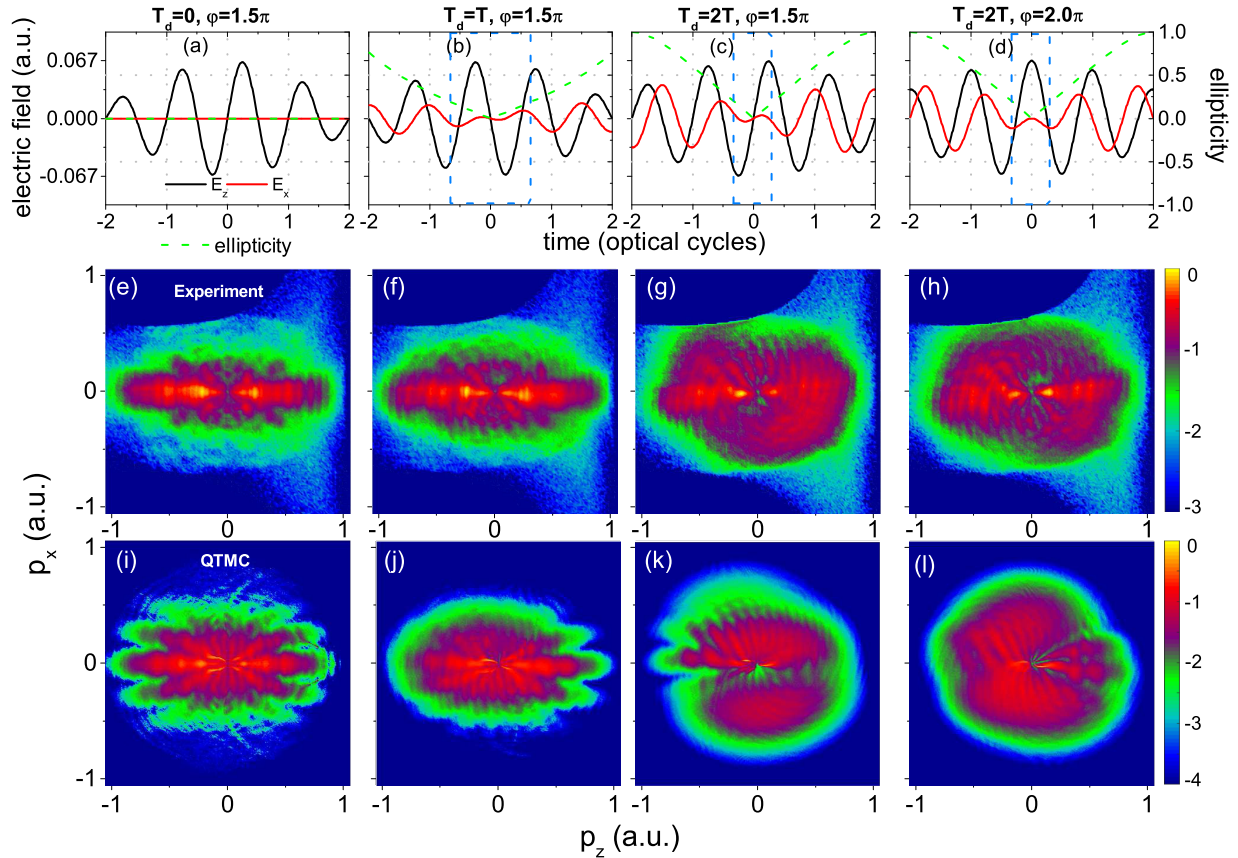


FIG. 2. (a)–(d) Electric-field components in the  $z$  and  $x$  directions and the ellipticity (green dash-dotted curve) of the PG pulses for different time delay and CEP combinations ( $T_d, \varphi$ ), (a) ( $0T, 1.5\pi$ ), (b) ( $1T, 1.5\pi$ ), (c) ( $2T, 1.5\pi$ ), and (d) ( $2T, 2.0\pi$ ), as a function of time. The peak intensity of the combined electric field is about  $1.5 \times 10^{14}$  W/cm<sup>2</sup>. (e)–(h) Measured PMDs of Ar ionized in the PG pulse with the same laser parameters as in (a)–(d), respectively. (i)–(l) Corresponding QTMC-simulated PMDs by sampling the EWPs within the whole PG pulse.

of various time delays and CEPs corresponding to Figs. 2(a)–2(d), respectively. The peak intensity of the combined laser field is about  $1.5 \times 10^{14}$  W/cm<sup>2</sup>. The sudden cutoffs of the photoelectron yield in the measured PMDs are due to the influence of the spectrometer magnetic field [46]. For  $\varphi = 1.5\pi$ , when  $T_d = 0$ , the PMD shows a pattern similar to that obtained with a linearly polarized driving field [36]. It exhibits a few ATI rings originating from the intercycle interference and a pronounced spiderlike structure that is produced by the interference between the direct and the forward-rescattering EWPs emitted within the same quarter cycle. The intracycle interferences are not visible since they are buried by these more prominent structures. When the time delay increases to  $1T$ , as shown in Fig. 2(f), the range of the distributed momentum in the  $p_x$  direction becomes larger since the transverse electric field starts to take effect in this case. Whereas the overall PMD for  $T_d = 1T$  shows characteristics, e.g., the spiderlike structure, similar to those for  $T_d = 0$ , when the time delay continues to increase to  $2T$ , the interference patterns in the measured PMD change significantly. As shown in Fig. 2(g), the ATI rings and the spiderlike structure have almost disappeared and a distinct interference pattern composed of a series of leftward curved stripes emerges in the upper part of the distribution (i.e.,  $p_x > 0$ ). Closer inspection

shows that the stripes in the  $p_x > 0$  plane gradually become thicker from right to left. In contrast to the spiderlike structure, these leftward curved stripes do not end at  $(p_x, p_z) = (0, 0)$ . We will discuss in the following that they are from intracycle interferences. On the other hand, in the  $p_x < 0$  plane, the PMD shows an interference pattern of circinate stripes. The interference patterns in the measured PMD are also dependent on the CEP of the PG pulse. As shown in Fig. 2(h), for  $T_d = 2T$ , when  $\varphi$  changes from  $1.5\pi$  to  $2.0\pi$ , some rightward curved stripes emerge in the  $p_x < 0$  plane, while the overall interference patterns in the PMD become somehow blurry.

To get physical insights into these experimental findings, we perform quantum-trajectory Monte Carlo (QTMC) simulations. Briefly, the QTMC theory describes the strong-field ionization semiclassically and fully considers the influence of the Coulomb potential while combining the Ammosov-Delone-Krainov theory [51] and Feynman's path-integral approach [52,53]. More details about the QTMC model can be found in Refs. [31,54]. In our simulations, the ionization yield is integrated over the spatiotemporal intensity distribution of the laser focus [55] to compare with the experimental measurement. The simulated results are shown in Figs. 2(i)–2(l), corresponding to the experimental data in Figs. 2(e)–2(h), respectively. All the simulated PMDs exhibit

rather good agreement with the experimental results. The interference patterns in both the simulated and measured PMDs show a strong dependence on the time delay and CEP. For the PG pulse with  $(2T, 1.5\pi)$ , both the simulated and measured PMDs exhibit a series of distinct leftward curved stripes in the  $p_x > 0$  plane and circinate stripes in the  $p_x < 0$  plane. It can be found that the photoelectron yields along  $p_x = 0$  are more significant for the measurements in Figs. 2(g) and 2(h) if compared to the corresponding QTMC simulations in Figs. 2(k) and 2(l). This might be attributed to the possible increase of pulse duration of each circularly polarized laser pulse due to dispersion. In the following we will seek to understand how the PG pulse with different time delays and CEPs affects the EWP interference and to reveal the origin of the interference patterns in the PMD for  $(2T, 1.5\pi)$ . To facilitate the analysis, the focus averaging effect is not considered in the following calculations.

#### IV. DISCUSSION

In general, the overall interference patterns observed in the PMD can be qualitatively understood with the simple man's model. In this model, the final photoelectron momentum after the laser pulse is given by  $\mathbf{p} = -\mathbf{A}(t_0)$ , where  $\mathbf{A}(t_0)$  is the laser field's vector potential at the emission time of  $t_0$  [56,57]. Figure 3(a) shows the laser field's vector potential components  $A_z(t_0)$  and  $A_x(t_0)$  for  $(2T, 1.5\pi)$ . In this case, both  $A_z(t_0)$  and  $A_x(t_0)$  are symmetric with respect to  $t_0 = 0$  and the periodicity of the laser pulse is broken in the central portion of the combined laser field. Thus the ATI ring structure will be strongly suppressed in the PMD. The simple man's mapping of electron emission time within  $L2$ ,  $L1$ ,  $R1$ , and  $R2$ , introduced in Fig. 3(a), to the final photoelectron momentum is depicted in Fig. 3(b). It can be deduced that the interference patterns in the PMD for  $(2T, 1.5\pi)$  are mainly caused by the EWPs emitted from the momentum-overlapped cycles  $L1$  and  $R1$ , since the EWPs emitted from  $L2$  and  $R2$  have relatively low yields and are mainly distributed in the momentum region of  $|p_x| > 0.5$  a.u. To understand the intracycle interferences within  $L1$  and  $R1$ , we depict in Fig. 3(c) the separate final PMDs of the EWPs emitted from the quarter cycles  $T1$ – $T8$  introduced in Fig. 3(a). Corresponding to  $A_x(t_0)$ , EWPs emitted from quarter cycles  $T1$ – $T4$  are mapped to the  $p_x > 0$  plane, whereas EWPs emitted from quarter cycles  $T5$ – $T8$  are mapped to the  $p_x < 0$  plane. Thus some kinds of interferences in the case of linearly polarized laser pulse, where  $A_x$  is zero, such as the interference from  $T4$  plus  $T7$  or  $T3$  plus  $T8$ , etc., will be strongly suppressed. As shown in Fig. 3(c), the final PMD predicted by the simple man's model in each quadrant mainly contains two kinds of EWPs emitted from different quarter cycles which are completely overlapped in momentum space, leading to distinct interference patterns observed in the measured PMD for  $(2T, 1.5\pi)$ . In Fig. 3(d) we also depict the separate final PMDs of the EWPs emitted from the quarter cycles  $T1$ – $T8$  for  $(2T, 2.0\pi)$ . In this case, EWPs emitted from different quarter cycles become separated from each other in the momentum space, which implies that it is more difficult for the EWP interferences to happen than in the case of  $\varphi = 1.5\pi$ . As a consequence, the interference patterns in the PMD become blurry.

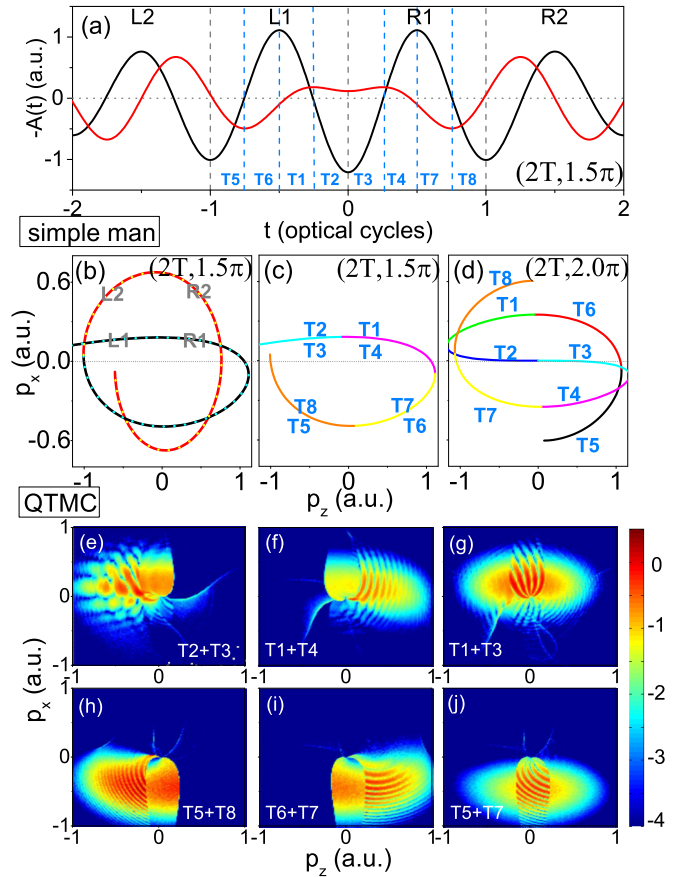


FIG. 3. (a) Laser field's vector potential components in the  $z$  (black curve) and  $x$  (red curve) directions for  $(2T, 1.5\pi)$ . The four dominated cycles are labeled  $L2$ ,  $L1$ ,  $R1$ , and  $R2$ . The center four quarter cycles are labeled  $T1$ – $T4$  and the neighboring four quarter cycles are labeled  $T5$ – $T8$ . Also shown is the simple man's prediction of the PMD,  $\mathbf{p} = -\mathbf{A}(t_0)$ , with  $t_0$  covering (b) the four-cycle central part of the PG pulse for  $(2T, 1.5\pi)$  and (c) and (d) the two-cycle central part of the PG pulse for (c)  $(2T, 1.5\pi)$  and (d)  $(2T, 2.0\pi)$ . (e)–(j) QTMC-simulated PMDs in logarithmic scale contributed by the EWPs emitted within different quarter cycles for  $(2T, 1.5\pi)$ . For more details, see the text.

Since the simple man's model cannot give detailed interference patterns in the PMD and does not consider the Coulomb potential effect, we further investigate the separate contributions of the quarter cycles  $T1$ – $T8$  to the overall PMD for  $(2T, 1.5\pi)$  using the QTMC simulations. Based on the simple man's mapping, the calculated PMDs by sampling EWPs emitted from adjacent quarter cycles  $T2$  plus  $T3$  and nonadjacent quarter cycles  $T1$  plus  $T4$  are shown in Figs. 3(e) and 3(f), respectively. Comparing Figs. 2(g) and 2(k) with Figs. 3(e) and 3(f), the origin of the leftward curved stripes in the PMD for  $(2T, 1.5\pi)$  becomes clear. In the  $p_x > 0$  plane, the thick leftward curved stripes in the second quadrant are due to the interference from adjacent quarter cycles  $T2$  plus  $T3$ , and the thin leftward curved stripes in the first quadrant are due to the interference from nonadjacent quarter cycles  $T1$  plus  $T4$ . Since EWPs emitted from  $T1$  plus  $T4$  have a longer ionization time delay compared with those emitted

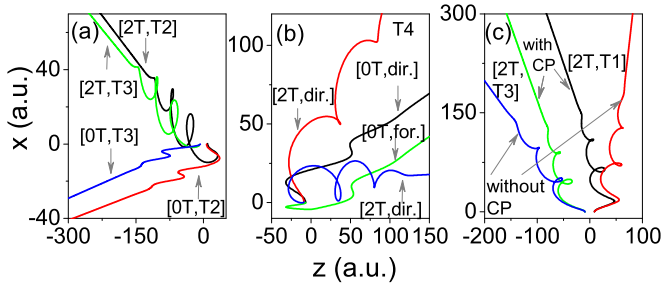


FIG. 4. Typical electron trajectories from the PG pulse with different time delays and emitted from different ionization time windows, labeled  $[T_d, T_n]$ , or with and without inclusion of the Coulomb potential (CP), as indicated in the figures. For comparison, the same initial conditions are chosen for two trajectories. See the text for details.

from  $T2$  plus  $T3$ , their interference stripes are much finer. In Fig. 3(e) we can also find a weak spiderlike structure, which is produced by the forward-rescattering PH interference [29] from quarter cycle  $T2$ . The suppression of the spiderlike structure in Fig. 3(e) could be attributed to the weakening of the Coulomb effect caused by the electron movement in the  $x$  direction. The spiderlike structure almost disappears in Fig. 3(f) because of larger ellipticity in  $T4$ . As shown in Fig. 3(g), besides the two kinds of intracycle interference structures predicted by the simple man's model, the leftward curved stripes around  $p_z = 0$  are produced by the interference from another two nonadjacent quarter cycles  $T1$  plus  $T3$ . We will explain in the following that this kind of interference is closely related to the residual Coulomb focusing effect of the ion. As demonstrated in the above discussion, three different types of intracycle interferences are clearly resolved and well separated in the  $p_x > 0$  plane of the PMD for  $(2T, 1.5\pi)$ . On the other hand, in the  $p_x < 0$  plane, as shown in Figs. 3(h)–3(j), it is clear that the circinate interference stripes observed in Fig. 2(g) are mainly contributed by the interferences from quarter cycles  $T5$  plus  $T8$  and  $T6$  plus  $T7$ , as predicted by simple man's model, and a new interference from quarter cycles  $T5$  plus  $T7$  caused by the Coulomb focusing effect, similar to the interference from quarter cycles  $T1$  plus  $T3$ .

To gain more insight into how the PG pulse controls the subcycle interference and disentangles different types of intracycle interferences for  $(2T, 1.5\pi)$ , we present in Figs. 4(a)–4(c) typical electron trajectories emitted from different quarter cycles. The electron trajectories, with the same initial conditions for  $(0T, 1.5\pi)$ , are also displayed for comparison. As shown in Fig. 4(a), when  $T_d = 0$ , corresponding to the case of a linearly polarized laser pulse, both electron trajectories, emitted from the quarter cycles  $T2$  and  $T3$ , drift in the  $p_x < 0$  direction. In contrast, when the time delay increases to  $2T$ , they are dragged by the electric field  $E_x$  to drift in the  $p_x > 0$  direction. Thus, the interference structure from  $T2$  plus  $T3$  will mainly be located in the  $p_x > 0$  plane for

$(2T, 1.5\pi)$ . In Fig. 4(b), for  $T_d = 0$ , we present direct (black curve) and forward-scattered (green curve) electron trajectories, both of which are emitted from  $T4$  with the same final momentum and lead to the spiderlike structure in the PMD. However, when the time delay increases to  $2T$ , the transverse electric field  $E_x$  makes the forward-scattered electron directly drift to the detector, and thus the two electron trajectories will not interfere with each other any longer. As a result, the spiderlike structure will be suppressed. In Fig. 4(c) we further present two typical trajectories emitted from the quarter cycles  $T1$  and  $T3$ , respectively. It clearly shows that the Coulomb potential will drag one of the electrons (black curve), ionized in the rising edge ( $T1$ ), to turn around in the  $z$  direction and drift to the detector in the same direction as another electron (green curve) that directly drifts to the detector. Thus, they will interfere with each other and give rise to the specific intracycle interference from the nonadjacent quarter cycles  $T1$  plus  $T3$ .

## V. CONCLUSION

We have experimentally demonstrated the feasibility of using a PG pulse to precisely control the intracycle interferences in the strong-field ionization process. We were able to resolve and separate distinctly several types of intracycle interferences in the PMDs with a PG pulse of  $T_d = 2T$  and  $\varphi = 1.5\pi$ . Using the simple man's and QTMC models, we explored how the PG pulse with different time delays and CEPs steer the intracycle interferences in the PMDs. Our analysis showed that the residual electric-field component in the transverse direction of the PG pulse plays an important role in separating various intracycle interferences in PMDs by properly distributing the interference stripes of electron wave packets, emitted within different time windows, into different momentum regions and suppressing the forward-rescattering PH interference. Our work will boost the PG technique as a powerful and universal tool to steer attosecond electron dynamics with high precision.

## ACKNOWLEDGMENTS

We thank Y. Q. Xu, H. Y. Sun, C. Z. Wan, Y. Wang, and Q. F. Chen for technical support of the laser system, electronic devices, and vacuum system. This work was supported by the National Key Research and Development Program of China (Grant No. 2019YFA0307702), National Natural Science Foundation of China (Grants No. 11834015, No. 11804374, No. 11874392, No. 11922413, No. 11974383, No. 12004391, No. 12004394, No. 12121004, and No. 12174401), Strategic Priority Research Program of the Chinese Academy of Sciences (Grant No. XDB21010400), China Postdoctoral Science Foundation (Grant No. 2019M662751), Youth Innovation Promotion Association CAS (Grant No. 2021328), the Science and Technology Department of Hubei Province (Grants No. 2019CFA035, No. 2020CFA029, and No. 2021CFA078), and K. C. Wong Education Foundation.

[1] C. J. Davisson and L. H. Germer, *Nature (London)* **119**, 558 (1927).

[2] G. P. Thomson and A. Reid, *Nature (London)* **119**, 890 (1927).

[3] C. Jönsson, *Z. Phys.* **161**, 454 (1961).

- [4] F. Lindner, M. G. Schätzel, H. Walther, A. Baltuška, E. Goulielmakis, F. Krausz, D. B. Milošević, D. Bauer, W. Becker, and G. G. Paulus, *Phys. Rev. Lett.* **95**, 040401 (2005).
- [5] J. Henkel, M. Lein, and V. Engel, *Phys. Rev. A* **83**, 051401(R) (2011).
- [6] J. Muth-Böhm, A. Becker, and F. H. M. Faisal, *Phys. Rev. Lett.* **85**, 2280 (2000).
- [7] Z. Y. Lin, X. Y. Jia, C. L. Wang, Z. L. Hu, H. P. Kang, W. Quan, X. Y. Lai, X. J. Liu, J. Chen, B. Zeng, W. Chu, J. P. Yao, Y. Cheng, and Z. Z. Xu, *Phys. Rev. Lett.* **108**, 223001 (2012).
- [8] M. Lein, N. Hay, R. Velotta, J. P. Marangos, and P. L. Knight, *Phys. Rev. Lett.* **88**, 183903 (2002).
- [9] T. Kanai, S. Minemoto, and H. Sakai, *Nature (London)* **435**, 470 (2005).
- [10] C. Vozzi, F. Calegari, E. Benedetti, J. P. Caumes, G. Sansone, S. Stagira, M. Nisoli, R. Torres, E. Heesel, N. Kajumba, J. P. Marangos, C. Altucci, and R. Velotta, *Phys. Rev. Lett.* **95**, 153902 (2005).
- [11] P. Liu, P. F. Yu, Z. N. Zeng, H. Xiong, X. C. Ge, R. X. Li, and Z. Z. Xu, *Phys. Rev. A* **78**, 015802 (2008).
- [12] M. Busuladžić, A. Gazibegović-Busuladžić, D. B. Milošević, and W. Becker, *Phys. Rev. Lett.* **100**, 203003 (2008).
- [13] T. Zuo, A. Bandrauk, and P. B. Corkum, *Chem. Phys. Lett.* **259**, 313 (1996).
- [14] C. I. Blaga, J. L. Xu, A. D. DiChiara, E. Sistrunk, K. K. Zhang, P. Agostini, T. A. Miller, L. F. DiMauro, and C. D. Lin, *Nature (London)* **483**, 194 (2012).
- [15] M. Meckel, D. Comtois, D. Zeidler, A. Staudte, D. Pavičić, H. C. Bandulet, H. Pépin, J. C. Kieffer, R. Dörner, D. M. Villeneuve, and P. B. Corkum, *Science* **320**, 1478 (2008).
- [16] M. Kunitski, N. Eicke, P. Huber, J. Köhler, S. Zeller, J. Voigtsberger, N. Schlott, K. Henrichs, H. Sann, F. Trinter, L. P. H. Schmidt, A. Kalinin, M. S. Schöffler, T. Jahnke, M. Lein, and R. Dörner, *Nat. Commun.* **10**, 1 (2019).
- [17] L. V. Keldysh, *Sov. Phys. JETP* **20**, 1307 (1965).
- [18] W. Becker, F. Grasbon, R. Kopold, D. B. Milošević, G. G. Paulus, and H. Walther, *Adv. At. Mol. Opt. Phys.* **48**, 35 (2002).
- [19] Y. Huismans, A. Rouzée, A. Gijsbertsen, J. H. Jungman, A. S. Smolkowska, P. S. W. M. Logman, F. Lépine, C. Cauchy, S. Zamith, T. Marchenko, J. M. Bakker, G. Berden, B. Redlich, A. F. G. van der Meer, H. G. Muller, W. Vermin, K. J. Schafer, M. Spanner, M. Y. Ivanov, O. Smirnova *et al.*, *Science* **331**, 61 (2011).
- [20] X. B. Bian and A. D. Bandrauk, *Phys. Rev. Lett.* **108**, 263003 (2012).
- [21] M. Meckel, A. Staudte, S. Patchkovskii, D. M. Villeneuve, P. B. Corkum, R. Dörner, and M. Spanner, *Nat. Phys.* **10**, 594 (2014).
- [22] Y. Zhou, O. I. Tolstikhin, and T. Morishita, *Phys. Rev. Lett.* **116**, 173001 (2016).
- [23] C. F. de Morisson Faria and A. S. Maxwell, *Rep. Prog. Phys.* **83**, 034401 (2020).
- [24] P. Agostini, F. Fabre, G. Mainfray, G. Petite, and N. K. Rahman, *Phys. Rev. Lett.* **42**, 1127 (1979).
- [25] R. R. Freeman and P. H. Bucksbaum, *J. Phys. B* **24**, 325 (1991).
- [26] D. G. Arbó, K. L. Ishikawa, K. Schiessl, E. Persson, and J. Burgdörfer, *Phys. Rev. A* **81**, 021403(R) (2010).
- [27] X. H. Xie, T. Wang, S. G. Yu, X. Y. Lai, S. Roither, D. Kartashov, A. Baltuška, X. J. Liu, A. Staudte, and M. Kitzler, *Phys. Rev. Lett.* **119**, 243201 (2017).
- [28] Y. L. Wang, S. G. Yu, X. Y. Lai, H. P. Kang, S. P. Xu, R. P. Sun, W. Quan, and X. J. Liu, *Phys. Rev. A* **98**, 043422 (2018).
- [29] D. D. Hickstein, P. Ranitovic, S. Witte, X. M. Tong, Y. Huismans, P. Arpin, X. Zhou, K. E. Keister, C. W. Hogle, B. Zhang, C. Ding, P. Johnsson, N. Toshima, M. J. J. Vrakking, M. M. Murnane, and H. C. Kapteyn, *Phys. Rev. Lett.* **109**, 073004 (2012).
- [30] M. Haertelt, X. B. Bian, M. Spanner, A. Staudte, and P. B. Corkum, *Phys. Rev. Lett.* **116**, 133001 (2016).
- [31] X. H. Song, J. W. Xu, C. Lin, Z. H. Sheng, P. Liu, X. H. Yu, H. T. Zhang, W. F. Yang, S. L. Hu, J. Chen, S. P. Xu, Y. J. Chen, W. Quan, and X. J. Liu, *Phys. Rev. A* **95**, 033426 (2017).
- [32] X. H. Xie, S. Roither, D. Kartashov, E. Persson, D. G. Arbó, L. Zhang, S. Grafe, M. S. Schöffler, J. Burgdörfer, A. Baltuska, and M. Kitzler, *Phys. Rev. Lett.* **108**, 193004 (2012).
- [33] M. Han, P. P. Ge, Y. Shao, M. M. Liu, Y. K. Deng, C. Y. Wu, Q. H. Gong, and Y. Q. Liu, *Phys. Rev. Lett.* **119**, 073201 (2017).
- [34] J. Tan, Y. M. Zhou, Q. H. Ke, M. R. He, J. T. Liang, Y. Li, M. Li, and P. X. Lu, *Phys. Rev. A* **101**, 013407 (2020).
- [35] R. Gopal, K. Simeonidis, R. Moshhammer, T. Ergler, M. Durr, M. Kurka, K. U. Kuhnel, S. Tschuch, C. D. Schroter, D. Bauer, J. Ullrich, A. Rudenko, O. Herrwerth, T. Uphues, M. Schultze, E. Goulielmakis, M. Uiberacker, M. Lezius, and M. F. Kling, *Phys. Rev. Lett.* **103**, 053001 (2009).
- [36] M. F. Kling, J. Rauschenberger, A. J. Verhoef, E. Hasović, T. Uphues, D. B. Milošević, H. G. Muller, and M. J. J. Vrakking, *New J. Phys.* **10**, 025024 (2008).
- [37] M. Richter, M. Kunitski, M. Schöffler, T. Jahnke, L. P. H. Schmidt, M. Li, Y. Q. Liu, and R. Dörner, *Phys. Rev. Lett.* **114**, 143001 (2015).
- [38] P. B. Corkum, N. H. Burnett, and M. Y. Ivanov, *Opt. Lett.* **19**, 1870 (1994).
- [39] Z. H. Chang, *Phys. Rev. A* **70**, 043802 (2004).
- [40] B. Shan, S. Ghimire, and Z. H. Chang, *J. Mod. Opt.* **52**, 277 (2005).
- [41] I. J. Sola, E. Mével, L. Elouga, E. Constant, V. Strelkov, L. Poletto, P. Villoresi, E. Benedetti, J. P. Caumes, S. Stagira, C. Vozzi, G. Sansone, and M. Nisoli, *Nat. Phys.* **2**, 319 (2006).
- [42] W. Quan, X. Liu, and C. Figueira de Morisson Faria, *J. Phys. B* **42**, 134008 (2009).
- [43] G. Sansone, E. Benedetti, F. Calegari, C. Vozzi, L. Avaldi, R. Flammini, L. Poletto, P. Villoresi, C. Altucci, R. Velotta, S. Stagira, S. De Silvestri, and M. Nisoli, *Science* **314**, 443 (2006).
- [44] T. Fuji, J. Rauschenberger, A. Apolonski, V. S. Yakovlev, G. Tempea, T. Udem, C. Gohle, T. W. Hänsch, W. Lehnert, M. Scherer, and F. Krausz, *Opt. Lett.* **30**, 332 (2005).
- [45] A. Baltuska, M. Uiberacker, E. Goulielmakis, R. Kienberger, V. S. Yakovlev, T. Udem, T. W. Hansch, and F. Krausz, *IEEE J. Sel. Top. Quantum Electron.* **9**, 972 (2003).
- [46] R. Dörner, V. Mergel, O. Jagutzki, L. Spielberger, J. Ullrich, R. Moshhammer, and H. Schmidt-Böcking, *Phys. Rep.* **330**, 95 (2000).
- [47] J. Ullrich, R. Moshhammer, A. Dorn, R. Dörner, L. P. H. Schmidt, and H. Schmidt-Böcking, *Rep. Prog. Phys.* **66**, 1463 (2003).
- [48] Y. L. Wang, S. P. Xu, W. Quan, C. Gong, X. Y. Lai, S. L. Hu, M. Q. Liu, J. Chen, and X. J. Liu, *Phys. Rev. A* **94**, 053412 (2016).

- [49] R. P. Sun, X. Y. Lai, S. G. Yu, Y. L. Wang, S. P. Xu, W. Quan, and X. J. Liu, *Phys. Rev. Lett.* **122**, 193202 (2019).
- [50] W. Quan, M. H. Yuan, S. G. Yu, S. P. Xu, Y. J. Chen, Y. L. Wang, R. P. Sun, Z. L. Xiao, C. Gong, L. Q. Hua, X. Y. Lai, X. J. Liu, and J. Chen, *Opt. Express* **24**, 23248 (2016).
- [51] M. V. Ammosov, N. B. Delone, and V. P. Krainov, *Sov. Phys. JETP* **64**, 1191 (1986).
- [52] R. P. Feynman, *Rev. Mod. Phys.* **20**, 367 (1948).
- [53] N. I. Shvetsov-Shilovski, M. Lein, L. B. Madsen, E. Räsänen, C. Lemell, J. Burgdörfer, D. G. Arbó, and K. Tökési, *Phys. Rev. A* **94**, 013415 (2016).
- [54] M. Li, J. W. Geng, H. Liu, Y. K. Deng, C. Y. Wu, L. Y. Peng, Q. H. Gong, and Y. Q. Liu, *Phys. Rev. Lett.* **112**, 113002 (2014).
- [55] R. Kopold, W. Becker, M. Kleber, and G. G. Paulus, *J. Phys. B* **35**, 217 (2002).
- [56] H. van Linden van den Heuvell and H. Muller, in *Proceedings of the Fourth International Conference on Multiphoton Processes, Boulder, 1987*, edited by S. J. Smith and P. L. Knight (Cambridge University Press, Cambridge, 1988), pp. 25–34.
- [57] P. B. Corkum, N. H. Burnett, and F. Brunel, *Phys. Rev. Lett.* **62**, 1259 (1989).